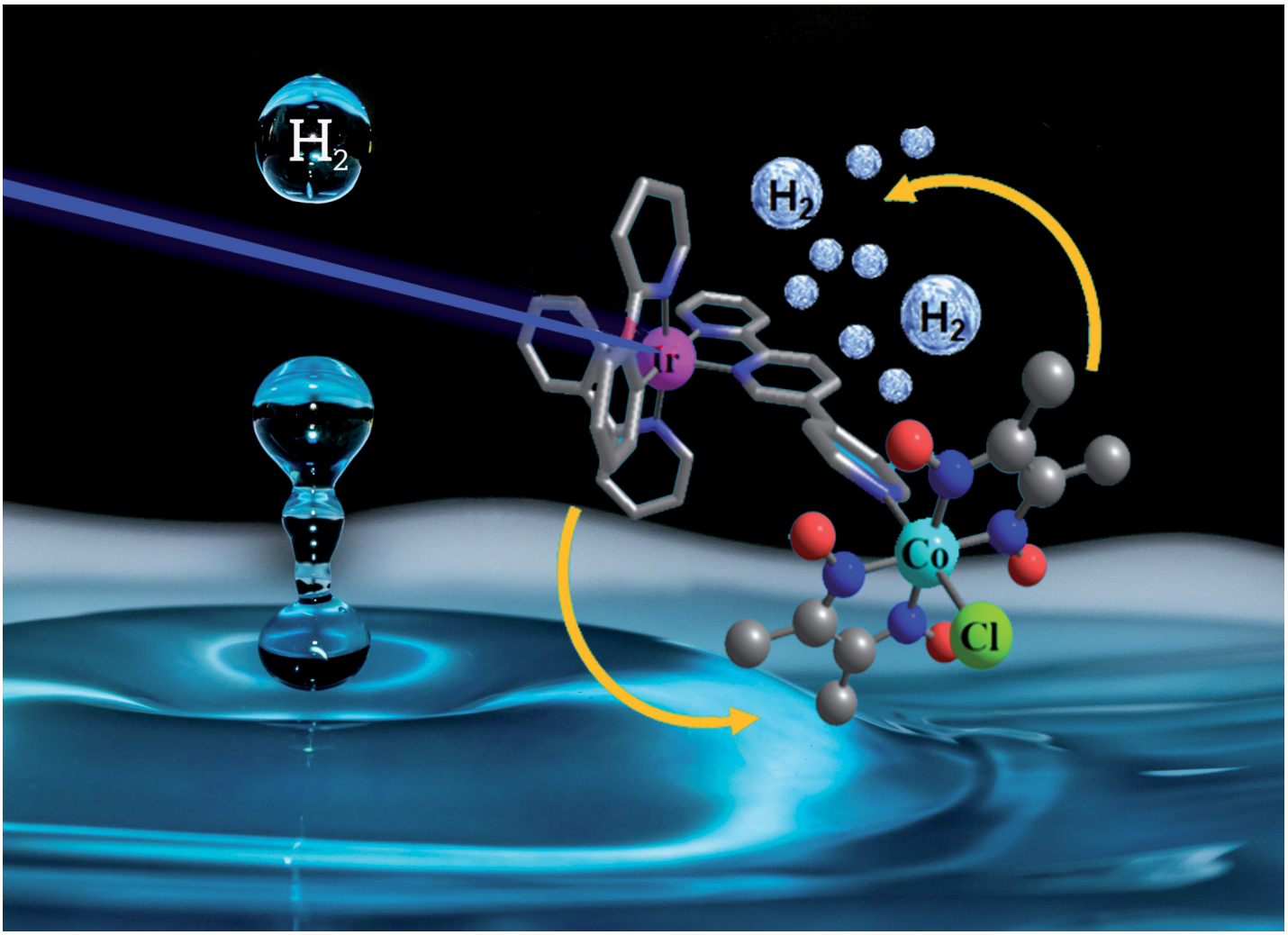

Showcasing research from Dr Moonshiram's and Dr Elias's laboratory, Instituto de Ciencia de Materiales de Madrid, Madrid, Spain and Institute of Condensed Matter and Nanoscience, Louvain-la-Neuve, Belgium

Deciphering the photophysical kinetics, electronic configurations and structural conformations of iridium–cobalt hydrogen evolution photocatalysts

Ultrafast optical and X-ray spectroscopies with time-dependent density functional theory reveal the electronic and structural conformations of Ir–Co hydrogen evolution photocatalysts. The results show the reaction pathways of versatile Ir–Co dyads important for future developments of earth-abundant photosensitizers for photocatalysis.

As featured in:

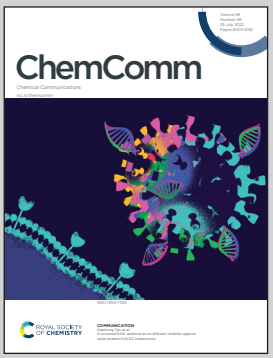

See Benjamin Elias, Dooshaye Moonshiram *et al.*, *Chem. Commun.*, 2022, **58**, 8057.

ROYAL SOCIETY OF CHEMISTRY

rsc.li/chemcomm

Registered charity number: 207890

ChemComm

COMMUNICATION

View Article Online
View Journal | View Issue

Cite this: *Chem. Commun.*, 2022, **58**, 8057

Received 21st April 2022,
Accepted 26th May 2022

DOI: 10.1039/d2cc02286a

rsc.li/chemcomm

Deciphering the photophysical kinetics, electronic configurations and structural conformations of iridium–cobalt hydrogen evolution photocatalysts†

Jiangyun Zhao,[a] Simon De Kreijger,[b] Ludovic Troian-Gautier,[b] Jin Yu,[c] Wenhui Hu,[d] Xiaoyi Zhang,[c] Benjamin Elias *[b] and Dooshaye Moonshiram *[a]

Picosecond optical and X-ray absorption spectroscopies with time-dependent density functional theory revealed the reaction pathways, electronic and structural conformations of Ir–Co hydrogen evolution photocatalysts. The dyad bearing 2-phenylpyridine ancillary ligands produced more photoreduced Co(II) than its 2-phenylisoquinoline analogue. These findings are important for designs of earth-abundant photosensitizers for photocatalytic applications.

In the face of today's rapid depletion of fossil fuels and emerging climate change crisis, alternative sustainable means of storing, transporting and distributing energy are being devised.[1] The abundant supply of solar energy provides an attractive means of storing energy through fuel forming reactions inspired by natural photosynthesis, such as the light induced splitting of water into molecular hydrogen and oxygen ($2H_2O + 4h\nu \rightarrow O_2 + 2H_2$).[2] The prospect of using molecular hydrogen as a carbon-free fuel has led to the rationalization and design of sustainable artificial molecular photosensitizer (PS)/catalytic assemblies where visible light is absorbed at the photosensitizer unit and converted into a chemical potential through charge accumulation processes at the catalytic unit. Recently, Ir–Co dyads (Scheme 1) consisting of cobaloxime hydrogen evolution catalysts $[Co(dmgH)(dmgH_2)]Cl_2$[3] ($dmgH_2$ = dimethylglyoxime) were chelated to Ir-based photosensitizers with 2-phenylpyridine ([Ir(ppy)$_2$-L]) (**dyad I**) or 2-phenylisoquinoline ([Ir(piq)$_2$-L]) ligands (**dyad II**) and found to display larger than 200 turnover rates of hydrogen generation upon light irradiation.[4] However key insights on the photo-induced electron transfer dynamics, photogenerated intermediates and influence of the cyclometalating ligands on the Ir-based photosensitizers that are responsible for the dyads' activities and essential for the fine-tuning of the light-harvesters' electronic properties were not investigated, yet are of crucial importance. In this regard, time-resolved X-ray (tr-XAS) and optical transient absorption (OTA) spectroscopies in the picosecond to microsecond time regime coupled with time-dependent density functional theoretical calculations (TD-DFT) are employed as powerful tools at both Co and Ir K and L-edges to extract valuable information about the coordination sphere around the cobalt catalytic centre and resolve the kinetics, electronic and structure scheme of these Ir-based photosensitizers.

Prior to performing time-resolved measurements, the cobaloxime-based Co^{III} catalyst and Ir-based photosensitizers were studied by X-ray absorption near edge structure (XANES) and Extended X-ray absorption fine structure (EXAFS). The XANES,

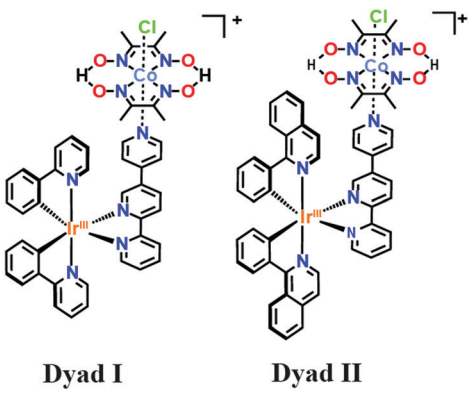

Scheme 1 Structure of the Ir–Co based **dyads I** and **II** obtained respectively through chelation of the Ir-based photosensitizers [Ir(ppy)$_2$-L] and [Ir(piq)$_2$-L] with the Co-based catalyst.

[a] *Instituto de Ciencia de Materiales de Madrid, Consejo Superior de Investigaciones Científicas, Sor Juana Inés de la Cruz, 3, 28049, Madrid, Spain. E-mail: dooshaye.moonshiram@csic.es*
[b] *Institute of Condensed Matter and Nanoscience, Molecular Chemistry, Materials and Catalysis Division, Place Louis Pasteur 1, Louvain-la-Neuve, Belgium. E-mail: benjamin.elias@uclouvain.be*
[c] *X-Ray Science Division, Argonne National Laboratory, 9700 South Cass Avenue, Lemont, IL 60439, USA*
[d] *Department of Chemistry, Marquette University, Milwaukee, WI 53201, USA*

† Electronic supplementary information (ESI) available: Experimental details, EXAFS fit analysis, XAS kinetic analysis, and results of DFT calculations. See DOI: https://doi.org/10.1039/d2cc02286a

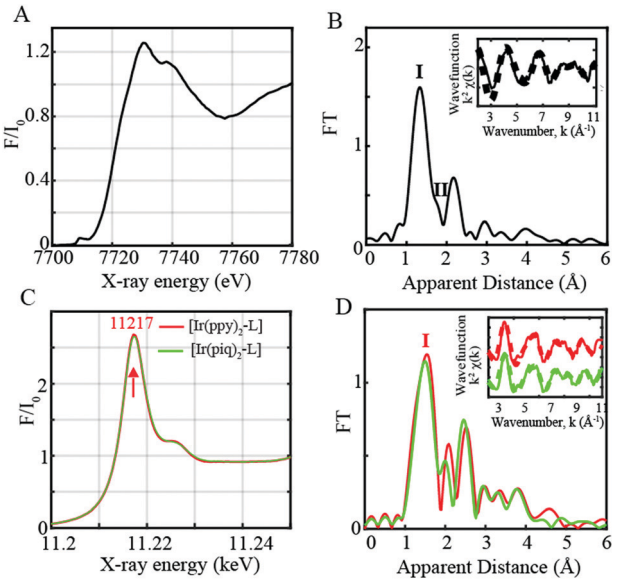

Fig. 1 (A) Normalized Co K-edge XANES for Co^{III} complex in **dyads I** and **II** (black). (B) Fourier transforms of k^2-weighted Co EXAFS for the Co catalyst (black). Inset: Back Fourier transformed experimental (solid lines) and fitted (dashed lines) $k_2[\chi(k)]$. (C) Normalized Ir L-edge XANES for $[Ir(ppy)_2\text{-L}]$ (red) and $[Ir(piq)_2\text{-L}]$ (green). (D) Fourier transforms of k^2-weighted Ir EXAFS Inset. Back Fourier transformed experimental (solid lines) and fitted (dashed lines) $k_2[\chi(k)]$ for Ir complexes in **dyads I** and **II**. Experimental spectra were calculated for k values of 2–11 $Å^{-1}$.

EXAFS and Fourier-transform (FT) of the k^2-weighted Co EXAFS spectra are shown in Fig. 1A, Fig. S1A (ESI†) and Fig. 1B respectively. A prominent peak and shoulder denoted as **Peaks I** and **II** (Fig. 1B) are observed in the Co^{III} FT EXAFS spectrum corresponding to the distinctive Co–N and Co–Cl bond distances. EXAFS fits for the first coordination sphere and the entire spectrum are shown in Fig. S2 and Table S1 in the ESI.† Analysis of the first peak in the cobaloxime Co^{III} complex clearly resolves 4 Co–N distances at 1.85 Å, and inclusion of a Co–Cl distance at 2.16 Å improves the quality of the fit as shown by the decreased R-factors and χ^2 value (Table S1, ESI,† Fits 1 and 3). The fitted Co–N and Co–Cl bond distances are in agreement with the reported XRD structure[4] and relaxed structures from DFT geometry optimization. Changes detected in experimental FT of the Co^{III} EXAFS further correlate well with data from X-ray diffraction (XRD) analysis and EXAFS simulations of DFT optimized coordinates (Fig. S3, ESI†).

The two Ir-based photosensitizers $[Ir(ppy)_2\text{-L}]$ and $[Ir(piq)_2\text{-L}]$ were further assessed through steady-state L-edge XANES and EXAFS spectroscopy (Fig. 1C, D and Fig. S1B, ESI†). Ir(III) complexes have a formal d_6 electronic configuration with filled t_{2g} and empty e_g levels. An intense peak corresponding to the Ir 2p to unoccupied 5d states with e_g symmetry is consequently observed at 11 217 eV (Fig. 1C) while no features are observed on the lower energy region below 11 217 eV due to the lack of vacancy in the t_{2g} states. The FT of the k^2-weighted $[Ir(ppy)_2\text{-L}]$ and $[Ir(piq)_2\text{-L}]$ EXAFS spectra display a prominent peak (**Peak I**, Fig. 1D) corresponding to the averaged Ir–N/C distances at 2.00 Å and 2.01 Å respectively, in close agreement with the reported XRD structures with Ir–N distances of 2.06 Å (Table S1 and Fig. S3, ESI†).

Following the steady-state measurements, tr-XAS was used to directly monitor the electronic conformations, kinetics and structural dynamics of the photo-generated Co^{II} and Ir triplet states in the supramolecular assemblies under photocatalytic conditions[4] with triethanolamine (TEOA) as the sacrificial electron donor and aqueous tetrafluoroboric acid as the proton source (Fig. 2 and 3). The Ir–Co binuclear dyads are optically pumped at 400 nm in the mixed Metal–Ligand-to-Ligand Charge Transfer (MLLCT) range with a 10 kHz repetition-rate laser and probed with X-ray pulses at several time delays from 100 ps to ~25 μs. XAS spectra of the supramolecular assemblies were collected before and after the laser excitation. By subtracting the laser-off from the laser-on spectrum, a transient signal is obtained for each pump-probe delay and provides information about the photo-induced dynamics, electronic and structural state of the catalyst's and photosensitizer's excited states.

Upon light excitation, mixed MLLCT from the 5 d orbital of Ir(III) to the π* orbital of the ligand followed by intersystem crossing (ISC) to a triplet excited state initially occurs.[5]

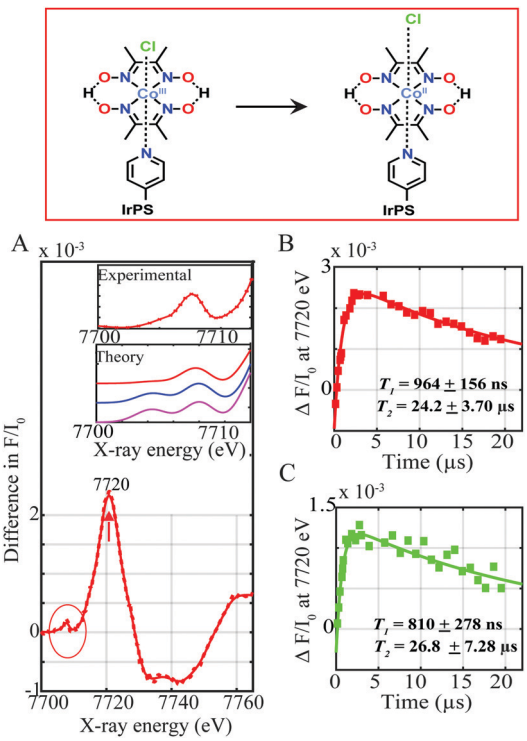

Fig. 2 (A) Experimental difference spectrum (laser on-laser off) corresponding to the Co^{III} transient signal at a time delay of ~11.3 μs between laser and X-ray pulses (red) in 1 mM **dyads I** and **II** with 1 M TEOA and 10 mM tetrafluoroboric acid. Inset. Zoom-in of the pre-edge Co^{II} transient experimental spectrum (red) (top) together with the simulated difference spectra for $[LCo^{II}Cl]^{2+}$ octahedral (red), $[LCo^{II}CH_3CN]^{2+}$ octahedral (blue) and $[LCo^{II}]^{2+}$ square pyramidal (magenta) geometries (bottom). Pump-probe time delay scans recorded at 7720 eV for (B) **dyad I** and (C) **dyad II**, reflecting the formation and decay of the Co^{II} photo-induced species. Kinetic fits T_1 and T_2 of the Co^{II} formation and decay processes are shown.

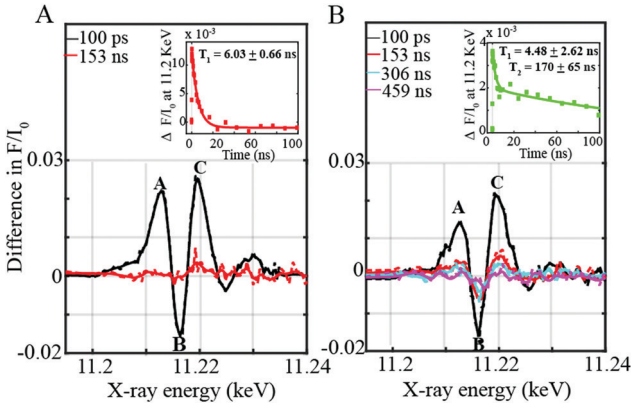

Fig. 3 Experimental difference spectra (laser on-laser off) corresponding to the ^{3}MLLCT signals of (A) [Ir(ppy)$_2$-L] and (B) [Ir(piq)$_2$-L] in **dyad I** and **II** respectively. Pump-probe time delay scans recorded at 11.2 keV of (A inset) [Ir(ppy)$_2$-L] in **dyad I** and (B inset) [Ir(piq)$_2$-L] in **dyad II** corresponding to the decay of the ^{3}MLLCT. Kinetic fits of the ^{3}MLLCT state's reaction with TEOA (T_1) with the excited-state relaxation time (T_2) for [Ir(piq)$_2$-L] due to inefficient quenching are indicated.

This process is followed by electron transfer from the excited photosensitizer to the Co^{III} complex, forming a Co^{II} species. Fig. 2A shows the Co tr-XAS spectrum of both supramolecular assemblies at an averaged time delay of 11.3 μs between laser and X-ray pulses. A prominent peak at 7720 eV together with a broad dip at 7735 eV is obtained which corresponds to the formation of the reduced Co^{II} species[6] and the ground state bleaching of the Co^{III}, respectively. These energy transitions in turn show that the K-edge of the Co centre shifts to lower energy, indicating the reduction of Co^{III} and confirming formation of Co^{II} through electron transfer from the Ir-based photosensitizers. Interestingly, clear changes are not only observed in the oxidation state of the Co catalytic metal site but also in its electronic configuration and coordination environment as indicated by the pre-edge region of the absorption spectrum at lower photon energies around 7710 eV (Fig. 2A inset, red trace).

Upon laser excitation, the occupation of the Co d shell changes from d^6 to d^7. The d level atomic rearrangements are accompanied by structure relaxation and hybridization of valence 3d states with N/O ligand p-orbitals.[7] It should be mentioned that the fractions of Co^{II} excited state between the laser pump excitation and X-ray probing were too low (less than 3%) to reconstruct the EXAFS and structural conformations of the excited states. Tr-XANES spectra were thus combined with TD-DFT XANES simulations to extract the electronic and geometric information about the photo-generated Co^{II} (Fig. 2A inset). Several possible geometries of the intermediate Co^{II} structure were theoretically explored. As shown from Fig. 2A inset, there is poor agreement between the experimental spectrum and theoretical simulation for a Co(II) square bipyramidal structure without any coordinated solvent molecules and an octahedral complex with a bonded acetonitrile molecule (compare red, blue and magenta traces). By contrast, the simulations for a distorted octahedral geometry with an elongated chlorido molecule at 2.4 Å resolve the pre-edge feature well (red trace) confirming the formation of a Co^{II} derivative with a loosely coordinated chloride in both supramolecular assemblies upon photoexcitation.

The kinetics for the formation and decay of the Co^{II} species were further investigated in both supramolecular assemblies by fixing the photon energy to 7720 eV, corresponding to the formation of Co^{II}, and varying the time delays between the laser and X-ray pulses (Fig. 2B and C and Fig. S4, ESI†). The formation and decay kinetics for the Co^{II} species are around the same in both dyads appearing promptly within 964 ± 154 ns and 810 ± 278 ns respectively (Fig. 2B and C), and decaying within 24.20 ± 3.70 μs and 26.80 ± 7.28 μs. Interestingly the Co transient signal of **dyad I** is around a factor of two greater than for **dyad II**, indicating more efficient formation of the Co^{II} reduced species (Fig. 2B and C).

In order to investigate this process further, time-resolved XANES were subsequently performed to elucidate the photo-induced electron transfer dynamics of the supramolecular assemblies at the Ir L-edge site. Three prominent features **I**, **II**, and **III** at energies of 11213, 11216 and 11220 eV respectively are observed (Fig. 3A and B). Feature **I** (Fig. 3A and B) corresponds to a 2p to Ir unoccupied t_{2g} state arising after electron transfer to the ligand.[8] Features **II** and **III** (Fig. 3A and B) by contrast appear due to an increase in the energy of the XANES white line upon photoexcitation. As previously corroborated through DFT calculations,[8] both the Ir 5d e_g and 2p states move towards lower energies in the photo-excited configuration of the triplet state. The shift of the 2p levels is however more significant than that of the 5d states resulting in an increase in the XANES white line[8] of the Ir-^{3}MLLCT state compared to the ground state thereby leading to a more positive feature **III** with a lower minimum feature **II** (Fig. 3A and B).

On the one hand, the ^{3}MLLCT state of the [Ir(ppy)$_2$-L] within the Ir–Co **dyad I** appears promptly within the 100 ps pulse duration of the X-ray and decays within 6.03 ± 0.66 ns (Fig. 3A inset). On the other hand, the transient spectrum of the [Ir(piq)$_2$-L] in Ir–Co **dyad II** persists within 100 ps to 459 ns time scales (Fig. 3B inset) and display 2 decay lifetimes of 4.48 ± 2.62 ns and 170 ± 65 ns. The Ir-based photosensitizers were further studied with TEOA in the absence of the Co-based catalyst and tetrafluoroboric acid, and similar time scales within error bars were obtained (Fig. S5, ESI†). Two electron-transfer pathways can exist for the photocatalytic cycle of the Ir–Co based supramolecular assemblies: (1) an oxidative quenching of the Ir photosensitizer ^{3}MLLCT state by the Co catalyst (2) a reductive quenching of the Ir photosensitizer by TEOA followed by electron transfer to the Co-based complex (Scheme 2). However, the oxidative quenching pathway can be ruled out as the Co-based catalyst is formed at much longer time scales of 810–960 ns than the decay of the Ir-based ^{3}MLLCT states as illustrated in Fig. 2B and C. Moreover, in the presence of excess TEOA employed as a sacrificial electron donor, the predominant pathway lies in the reductive quenching of the Ir ^{3}MLLCT. The decay lifetime T_1 of 4.48–6.02 ns observed in both dyads consequently corresponds to the formation of the reduced ^{3}MLLCT state as illustrated in Scheme 2. Importantly,

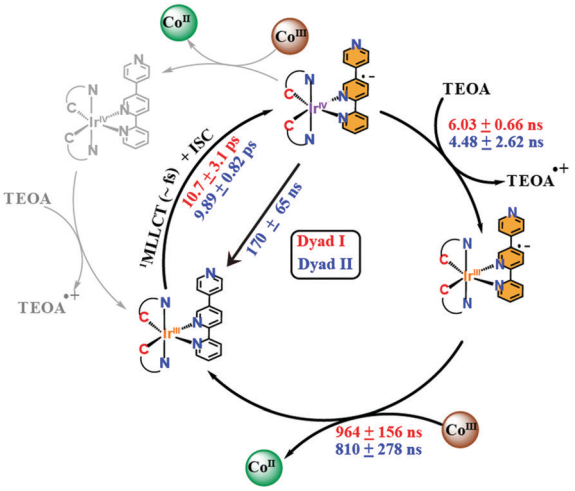

Scheme 2 Mechanistic pathways of Ir–Co **dyads I** and **II**. Rate constants for **dyads I** and **II** are respectively shown in red and blue.

the 2nd decay lifetime T_2 of 170 ± 65 ns obtained for the [Ir(piq)$_2$-L] photosensitizer in both the absence and presence of the Co-based catalyst corresponds to the decay to the Ir(III) ground state due to inefficient quenching. This is further corroborated by the low excited state fraction obtained for the Ir–Co **dyad II**. Around 50% of the [Ir(piq)$_2$-L] recombines back to the ground state configuration while only the other 50% participates in the efficient electron transfer reaction to the Co^{III} catalyst to generate the photo-reduced Co^{II} species (Fig. 2C).

Finally, limited by the 100 ps pulse duration of the X-rays, the ISC time frame from the singlet to the triplet excited states as well as the decay of the ^{3}MLLCT states of the Ir-based photosensitizers within both dyads, were determined through OTA from 1 ps to 2 ns time scales (Fig. S6, ESI†).

Interestingly, [Ir(ppy)$_2$-L] and [Ir(piq)$_2$-L] display similar ISC times within experimental errors, *i.e.* 10.7 ± 3.1 ps and 9.89 ± 0.82 ps respectively (Fig. S6A and B, ESI†). Similarly, the ^{3}MLLCT states for [Ir(ppy)$_2$-L] and [Ir(piq)$_2$-L] in **dyads I** and **II** decay within 7.74 ± 1.71 ns and 6.68 ± 0.19 ns (Fig. S6A and B, ESI†) respectively, consistent with the decay lifetimes of the ^{3}MLLCT states of the Ir-based photosensitizers obtained through tr-XAS (Fig. 3A and B inset).

Despite their similarities, [Ir(ppy)$_2$-L] and [Ir(piq)$_2$-L] bear different electron densities leading to their varying photophysical properties. Previous TD-DFT calculations[4] has showed that the lowest triplet excited state for [Ir(ppy)$_2$-L] is a ^{3}MLLCT state while that for [Ir(piq)$_2$-L] consists of a combination of C^N centred and ^{3}LC characters. The increased contribution of the ^{3}LC transition on the excited state conformation of [Ir(piq)$_2$-L] leads to a lesser efficient ^{3}MLLCT state and a lower electron density in the excited state of the pendant pyridine moiety thus causing rapid decay to the ground state as revealed from tr-XAS measurements conducted in the presence and absence of the Co catalyst (Fig. 3B inset and Fig. S5B, ESI†). Hydrogen evolution measurements previously carried out[4] under similar experimental conditions as tr-XAS with triethanolamine as sacrificial electron donor and tetrafluoroboric acid as the proton source further showed that **dyads I** and **II** displayed maximum turnover frequency (TOF) of 180 and 58 under green light excitation thus corroborating the decreased efficiency of [Ir(piq)$_2$-L].

In summary, combined OTA and tr-XAS measurements at Co K-edge and Ir L-edge energies with DFT calculations were systematically employed to evaluate the influence of the 2-phenylpyridine and 2-phenylisoquinoline ligands on Ir-based photosensitizers when chelated to a Co-based hydrogen evolution catalyst (Scheme 2). Time-resolved XANES with TD-DFT simulations at the Co K-edge shows that upon photoexcitation, the Co^{III} octahedral catalyst is reduced to a Co^{II} species and undergoes a Co–Cl bond elongation (Fig. 2A). We additionally monitored the rise time kinetics of the Co^{II} intermediate in both dyads to be 810–964 ns followed by its decay to form the starting Co^{III} complex within 24.2–26.8 μs (Fig. 2B and C). The study of the supramolecular assemblies at the Ir L-edge showed the prompt formation of an Ir ^{3}MLLCT state within the 100 ps pulse duration of the X-rays in both dyads (Fig. 3A and B). Further, combined kinetics studies through OTA and Ir L-edge tr-XAS conclusively reveal that both Ir-based photosensitizers in **dyads I** and **II** have similar ISC times of 9.89–10.7 ps and are reductively quenched by TEOA within 4.48–7.74 ns (Fig. 3A and B inset and Fig. S6, ESI†). Importantly, [Ir(piq)$_2$-L] in **dyad II** is found to be less efficient than its [Ir(ppy)$_2$-L] counterpart in **dyad I** as it not only displays decay to the Ir^{III} ground state within 170 ± 65 ns (Fig. 3B and 2C) but additionally illustrates 50% less electron transfer efficiency to the Co^{III} catalyst to generate the photoreduced species. This study provides important insights on the reaction pathways and efficiencies of a family of highly versatile supramolecular Ir–Co dyads and holds future promise for the improved developments of both Ir-based and earth-abundant photosensitizers with lesser conjugated cyclometalated ligand derivatives for photocatalytic applications.

Conflicts of interest

There are no conflicts to declare.

Notes and references

1 D. G. Nocera, *Acc. Chem. Res.*, 2011, **45**, 767–776.
2 N. Armaroli and V. Balzani, *Angew. Chem., Int. Ed.*, 2007, **46**, 52–66.
3 J. L. Dempsey, B. S. Brunschwig, J. R. Winkler and H. B. Gray, *Acc. Chem. Res.*, 2009, **42**, 1995–2004.
4 C. Lentz, O. Schott, T. Auvray, G. S. Hanan and B. Elias, *Dalton Trans.*, 2019, **48**, 15567–15576.
5 R. Bevernaegie, S. A.-M. Wehlin, B. Elias and L. Troian-Gautier, *ChemPhotoChem*, 2021, **5**, 217–234.
6 D. Moonshiram, C. Gimbert-Suriñach, A. Guda, A. Picon, C. S. Lehmann, X. Zhang, G. Doumy, A. M. March, J. Benet-Buchholz, A. Soldatov, A. Llobet and S. H. Southworth, *J. Am. Chem. Soc.*, 2016, **138**(33), 10586–10596.
7 T. E. Westre, P. Kennepohl, J. G. DeWitt, B. Hedman, K. O. Hodgson and E. I. Solomon, *J. Am. Chem. Soc.*, 1997, **119**, 6297–6314.
8 G. Smolentsev, K. M. van Vliet, N. Azzaroli, J. A. van Bokhoven, A. M. Brouwer, B. de Bruin, M. Nachtegaal and M. Tromp, *Photochem. Photobiol. Sci.*, 2018, **17**, 896–902.

